Article

Cell Systems

Stochastic modeling of single-cell gene expression adaptation reveals non-genomic contribution to evolution of tumor subclones

Graphical abstract

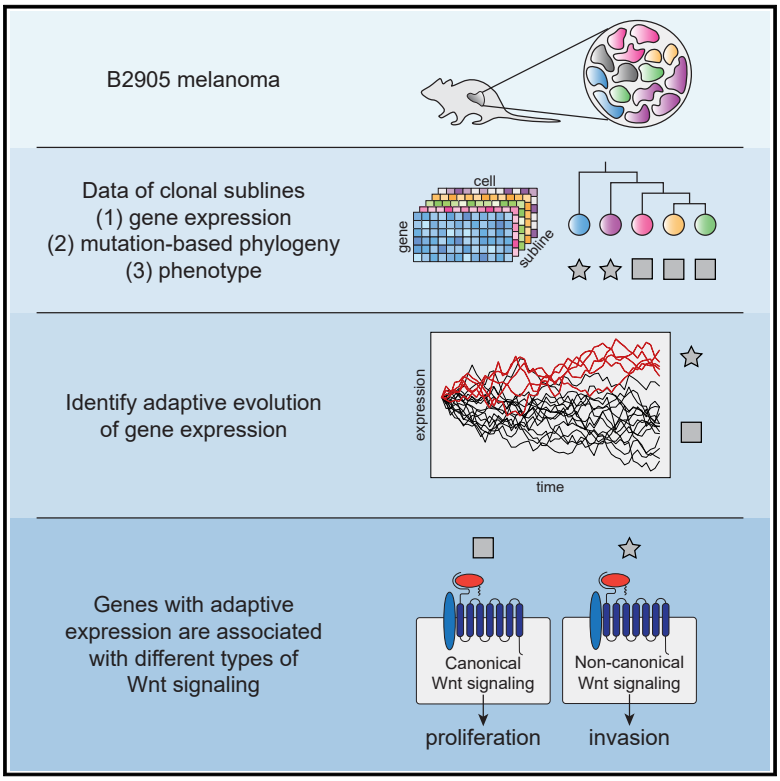

Highlights

- Stochastic modeling identifies genes with adaptive expression
- Adaptation results in proliferative and invasive phenotypes of subclones
- Subclones that adapt for canonical Wnt signaling are sensitive to immunotherapy
- Subclones that adapt for non-canonical Wnt signaling are resistant to immunotherapy

Authors

M.G. Hirsch, Soumitra Pal, Farid Rashidi Mehrabadi, ..., Erin K. Molloy, Chi-Ping Day, Teresa M. Przytycka

Correspondence

daychi@nih.gov (C.-P.D.), przytyck@ncbi.nlm.nih.gov (T.M.P.)

In brief

This study uses a stochastic model of gene expression evolution to study evolutionary adaptation in melanoma subclones with distinct phenotypes. It uncovers distinct adaptive gene expression patterns associated with canonical and non-canonical Wnt signaling, resulting in the proliferative and invasive melanoma phenotypes, respectively.

Hirsch et al., 2025, Cell Systems *16*, 101156
January 15, 2025 Published by Elsevier Inc.
https://doi.org/10.1016/j.cels.2024.11.013

CellPress

Cell Systems

CellPress
OPEN ACCESS

Article

Stochastic modeling of single-cell gene expression adaptation reveals non-genomic contribution to evolution of tumor subclones

M.G. Hirsch,[1,2] Soumitra Pal,[3] Farid Rashidi Mehrabadi,[4,5] Salem Malikic,[4] Charli Gruen,[6] Antonella Sassano,[6] Eva Pérez-Guijarro,[6,7] Glenn Merlino,[6] S. Cenk Sahinalp,[4] Erin K. Molloy,[2,8] Chi-Ping Day,[4,*] and Teresa M. Przytycka[1,9,*]

[1]National Library of Medicine (NLM), National Institutes of Health (NIH), Bethesda, MD 20892, USA
[2]Department of Computer Science, University of Maryland, College Park, MD 20742, USA
[3]Neurobiology Neurodegeneration and Repair Lab, National Eye Institute (NEI), National Institutes of Health (NIH), Bethesda, MD 20892, USA
[4]Cancer Data Science Laboratory, Center for Cancer Research, National Cancer Institute (NCI), National Institutes of Health (NIH), Bethesda, MD 20892, USA
[5]Laboratory of Human Carcinogenesis, Center for Cancer Research, National Cancer Institute (NCI), National Institutes of Health (NIH), Bethesda, MD 20892, USA
[6]Laboratory of Cancer Biology and Genetics, Center for Cancer Research, National Cancer Institute (NCI), National Institutes of Health (NIH), Bethesda, MD 20892, USA
[7]Instituto de Investigaciones Biomédicas Sols-Morreale, Consejo Superior de Investigaciones Científicas, Universidad Autónoma de Madrid (IIBM, CSIC-UAM), Madrid 28029, Spain
[8]University of Maryland Institute for Advanced Computer Studies, College Park, MD 20742, USA
[9]Lead contact
*Correspondence: daychi@nih.gov (C.-P.D.), przytyck@ncbi.nlm.nih.gov (T.M.P.)
https://doi.org/10.1016/j.cels.2024.11.013

SUMMARY

Cancer progression is an evolutionary process driven by the selection of cells adapted to gain growth advantage. We present a formal study on the adaptation of gene expression in subclonal evolution. We model evolutionary changes in gene expression as stochastic Ornstein-Uhlenbeck processes, jointly leveraging the evolutionary history of subclones and single-cell expression data. Applying our model to sublines derived from single cells of a mouse melanoma revealed that sublines with distinct phenotypes are underlined by different patterns of gene expression adaptation, indicating non-genetic mechanisms of cancer evolution. Sublines previously observed to be resistant to anti-CTLA4 treatment showed adaptive expression of genes related to invasion and non-canonical Wnt signaling, whereas sublines that responded to treatment showed adaptive expression of genes related to proliferation and canonical Wnt signaling. Our results suggest that clonal phenotypes emerge as the result of specific adaptivity patterns of gene expression. A record of this paper's transparent peer review process is included in the supplemental information.

INTRODUCTION

Cancer refers to a spectrum of diseases in which cells acquire the ability to evade normal mechanisms that control cell growth, differentiation, and movement. It is generally assumed that cancer originates from a single cell (or a small number of cells) and progresses through a branched evolutionary process during which cells can acquire new mutations, undergo epigenetic reprogramming, and differentiate into distinct heterogeneous subpopulations, referred to as subclones. This clonal evolutionary process is generally assumed to be driven by the selection of cells exhibiting properties related to growth advantage, like immunoevasion, evasion of cell death, and cell growth.[1–3] Understanding these selective forces is important, yet studies investigating them have been limited and mutation-centric.[4,5] While mutations are fundamental to many aspects of cancer studies, their impact on cell function is often indirect, and cancer evolution also proceeds by epigenetic changes.[6–8] A more direct way to uncover selective trends in tumor evolution due to the combined effect of genetic and non-genetic factors is to study adaptive changes in gene expression because changes in gene expression mostly cause direct alteration of cell functions. Studying the evolutionary pressures acting on gene expression in light of clonal evolution can provide critical insights into the molecular changes that confer fitness advantage. Molecular changes caused by gene expression adaptation also impact response to specific therapies that modulate the gene expression, and thus the functions, of cells. Knowledge of the evolution of gene expression can then enable the design of more effective treatment protocols.

Until recently, the ability to investigate such selective processes has been limited because of the use of bulk sequencing,

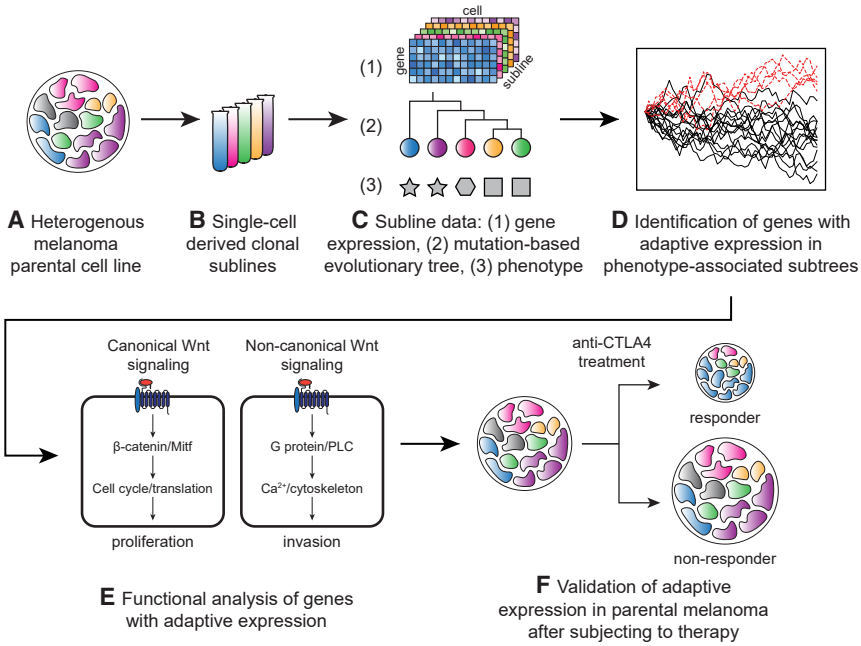

Figure 1. Summary of approach

A heterogeneous melanoma cell line (A) is used to obtain single-cell-derived sublines (B). Single-cell gene expression data, a mutation-based phylogenetic tree, and phenotypic features of the tumors derived from the sublines (C) are used to identify genes with adaptive expression associated with the cancer phenotypes (D). The genes with adaptive expression are subjected to functional analysis (E). For additional validation, tumors seeded from the parental line are subjected to anti-CTLA4 treatment. Overlap between genes with adaptive expression and genes differentially expressed between post-treatment responder and non-responder tumors is compared (F). Colors in (A)–(C) and (F) represent different subclones/sublines. Colors in (D) represent the phenotypes each subline.

which cannot differentiate between cell-level selection and expression changes due to changes in cell populations. Single-cell RNA sequencing, on the other hand, gives us the opportunity to study gene expression evolution both within and across subclones, which otherwise is obfuscated when using bulk data. Single-cell RNA sequencing has been increasingly utilized to study dynamical changes in cell populations. Methods taking advantage of single-cell RNA sequencing include pseudotime analysis methods, which order cells along a trajectory based on similarities in their expression patterns (reviewed in Saelens et al.[9]), and RNA velocity approaches, which employ splicing information to infer directed cellular changes.[10] Single-cell data have also been used with Ornstein-Uhlenbeck (OU) processes in order to investigate gene expression changes throughout cellular differentiation.[11] These methods are key in understanding the cellular differentiation process, but they do not investigate changes at extended evolutionary scales.

Other methods that examine longer time frames use gene expression to identify clusters of tumor cells that comprise different subclones. They then perform differential expression analysis between the clusters to identify genes with expression that vary between the subclones.[12–14] However, not only are relationships between such clusters and tumor subclones often complex,[15] but differential expression methods give no information about whether the difference in gene expression is due to selective pressures or neutral evolution over diversifying evolutionary distances.[16]

Here, we perform a formal study directly modeling evolutionary shifts on gene expression caused by selective pressures within the tumor microenvironment. Specifically, we leverage single-cell full-length RNA sequencing data to investigate the role of selection on gene expression and function in the subclonal evolution of cancer. We model clonal gene expression evolution using stochastic OU processes, which have been previously applied in the context of species evolution[13,17–22] and cellular differentiation,[11] but have not been utilized in studies on subclonal evolution. Our use of OU processes allows us to model changes in subclone-specific expression along trajectories defined by the evolutionary history of the subclones. Utilizing the evolutionary history enables us to evaluate whether gene expression is shifting because it is subject to adaptive evolution as opposed to shifting due to random changes caused by neutral evolution. Further, using single-cell data allows us to distinguish between subclonal growth and adaptive evolution, which is critical to understanding selective pressures in cancer and is not possible with differential expression analysis, even when clusters accurately reflect subclones.

To evaluate the capabilities and limitations of the OU processes, we first evaluated the performance of the models on realistic simulations of single-cell RNA tumor evolution data. We then used the OU processes to model the evolution of the M4 melanoma,[1] which exhibited intratumoral heterogeneity[23] (Figure 1). Specifically, we applied these stochastic processes on multiple "clonal sublines" of an M4 melanoma cell line (known as B2905)[2] (Figures 1A and 1B). In our analysis, we incorporated knowledge of the evolutionary history of the sublines based on their mutations and their phenotypes, such as aggressiveness and immunogenicity (Figure 1C), and identified genes with adaptive expression related to these phenotypes (Figure 1D). We found that different phenotypes were associated with adaptation of gene expression for distinct genes and pathways. Included in these pathways were alternative Wnt signaling pathways, implying an association between clonal selection for alternative Wnt signaling and immune response (Figure 1E). By subjecting the parental M4 melanoma to anti-CTLA4 treatment, we further found that genes with adaptive expression in the treatment-resistant sublines captured by our analysis display expression in post-treatment tumors consistent with immunotherapy response (Figure 1F).

Our study provides evidence that evolution of distinct phenotypes in cancer is driven by selection of subclones based on gene expression. We use single-cell RNA sequencing, a mutation-based phylogeny, and phenotypic information for evaluating

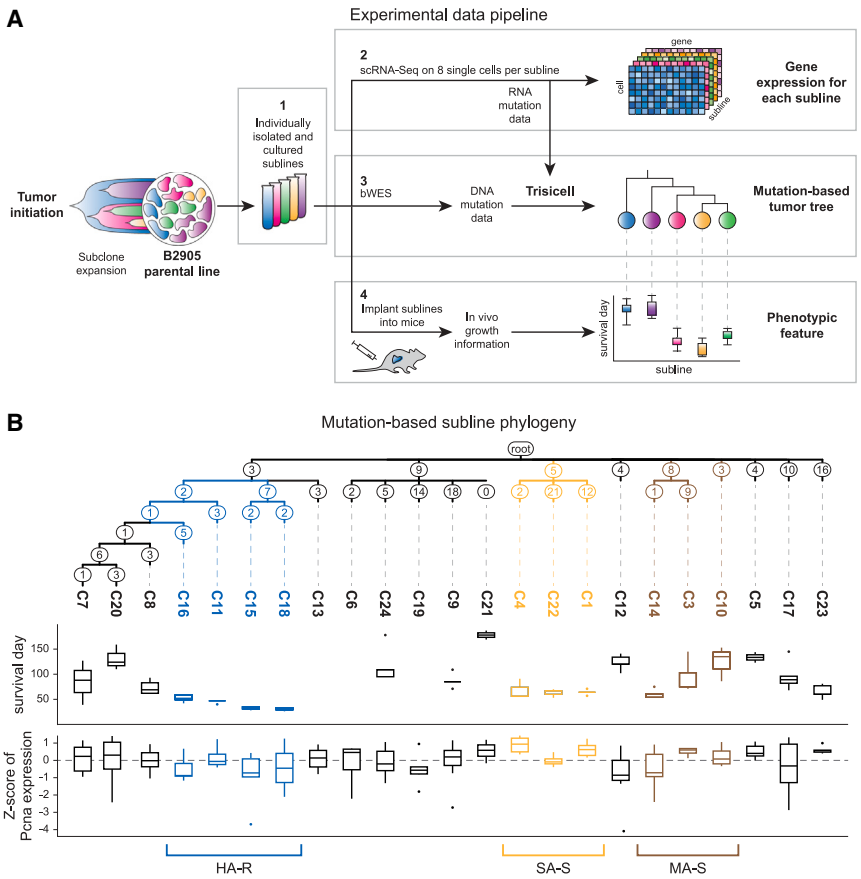

Figure 2. Experimental data of subclonal evolution in a mouse melanoma

(A) Schematic illustrating the generation of the clonal sublines from a mouse melanoma cell line. Box 1: 24 single cells are isolated from the parental B2905 cell line and cultured into sublines. Only five shown for illustration purposes. Box 2: the sublines undergo single-cell RNA sequencing, resulting in gene expression data for each subline. Box 3: the sublines undergo bulk whole-exome sequencing and mutation calling. The mutation data are used to create a mutation-based tumor tree using Trisicell.[15] Box 4: the individual sublines are implanted into mice and allowed to grow. *In vivo* growth information for each subline-derived tumor is recorded, resulting in distinct phenotypes (time to reach a pre-defined size) across sublines. Colors represent different subclones/sublines.

(B) Consensus mutation-based phylogenetic tree estimated by Trisicell, growth kinetics, and *Pcna* expression of the clonal sublines.[15] The branches are labeled with the number of expressed mutations along that branch, which are used as the branch lengths of the phylogeny. Sublines are colored based on their phenotypes: HA-R sublines (C11, C15, C16, and C18) are blue, SA-S sublines (C1, C4, and C22) are orange, and MA-S sublines (C3, C10, and C14) are brown. Growth kinetics, measured in the time the tumor took to reach a predefined size, are shown in the first row below each subline. Sublines that did not reach the set tumor size in the time frame have no growth kinetics shown. The second row below each subline shows the *Z* score of the log_2 expression of *Pcna*. The *Z* score has the same distribution as the expression but centers the mean at zero for easier comparison. Positive values mean the subline has higher expression of *Pcna* than the mean, and negative values mean the subline has lower expression than the mean.

evolutionary selective forces acting on gene expression. Such analysis could inform targeted treatment for tumors exhibiting different phenotypes to increase the efficacy of the treatment and decrease the chance of tumor recurrence.

RESULTS

Gene expression adaptation of clonal evolution in cancer can be modeled with OU processes applied to single-cell RNA (scRNA) data

Experimental setting

To study gene expression evolution in cancer, we analyze data that were previously generated in Gruen et al.,[24] and here, we briefly review the data generation protocol. When implanted in syngeneic C57BL/6 mice, B2905 melanoma cells form tumors that exhibit heterogeneous responses to immune checkpoint blockade (ICB) therapies among individual hosts.[23] To reconstruct the subclonal evolutionary history of the melanoma, 24 single cells were first isolated from the parental B2905 cell line and expanded to become individual clonal sublines, C1 to C24 (Figure 2A; box 1), as described previously.[24] The sublines represent subclones derived from the melanoma cell of common origin. The sublines were then subjected to bulk whole-exome sequencing (bWES) (Figure 2A; box 3). Mutations were called from the exome data and used to build a phylogeny of the sublines. Next, for each subline, eight cells were isolated for full-length single-cell RNA sequencing (Figure 2A; box 2). Cells were filtered based on quality control measures (see STAR Methods), leaving one to eight gene expression measurement replicates per subline. Subline C2 is excluded from further analysis due to technical reasons,[15] leaving 23 sublines for analysis. Mutations were also called from the single-cell RNA data and used to build a second phylogeny of the sublines. A consensus tree was constructed between the DNA and RNA mutation-based phylogenies as described in Rashidi Mehrabadi et al.,[15] and this tree is what is used in this study (Figure 2B).

Cells from the individual sublines were then implanted into distinct but genetically identical mice, and *in vivo* growth information was recorded (Figure 2A; box 4). In their original analysis of the data, Rashidi Mehrabadi et al.[15] found that sublines of major clades in the phylogeny exhibited distinct growth kinetics *in vivo* (measured by the survival time of the hosts following implantation of the cells to grow tumors; Figure 2B) and/or putative sensitivity to ICB treatment.

We identify two groups of sublines that have particularly fast growth rates: C11, C15, C16, and C18, which have the fastest

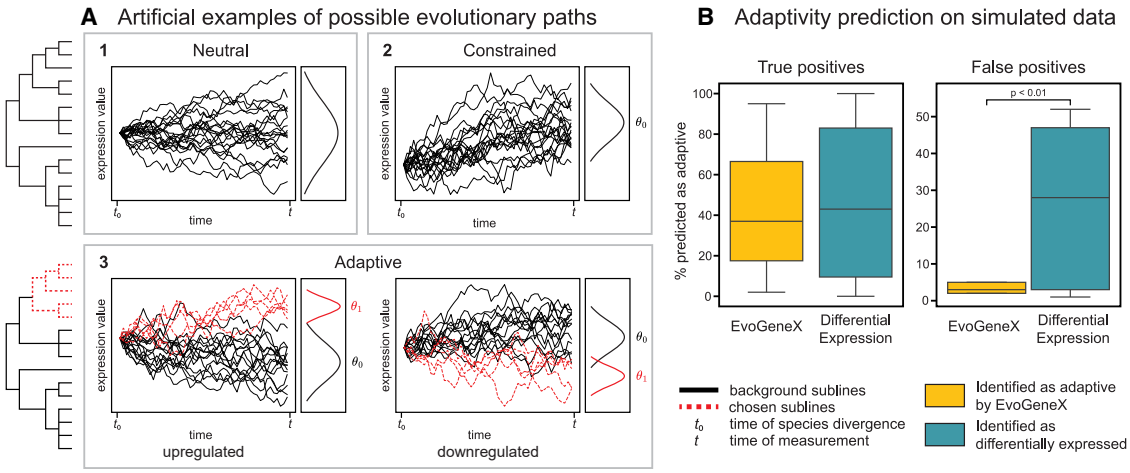

Figure 3. Simulated identification of genes with adaptive expression by OU process

(A) Examples of possible evolutionary trajectories of gene expression along the phylogeny. On the left is the phylogeny that was used to simulate the data. For neutral (box 1) and constrained (box 2) evolution, no phenotypic feature is used, and all sublines are considered to have the same dynamics (solid black branches). In adaptive evolution (box 3), some sublines have different evolutionary dynamics (dashed red branches). Each box shows a simulated example evolutionary trajectory of expression for the different sublines as well as the resulting expression distribution that would be observed and used as input to the model. Optima values (θ) used to simulate the data are indicated where applicable.

(B) Adaptivity and differential expression predictions on data simulated under a negative binomial distribution. Right: percentage of adaptively simulated genes for each of the 135 parameter combinations correctly identified to be adaptive or differentially expressed across all simulations. Left: percentage of neutrally simulated genes for each of the 9 parameter combinations incorrectly identified to be adaptive or differentially expressed across all simulations (difference is statistically significant with independent t test p value < 0.01). Results from EvoGeneX are shown in yellow; results from differential expression are shown in teal. See STAR Methods for details on simulation simulations.

growth rates, and C1, C22, and C4, which have the second fastest growth rates, consistent with the classifications in Rashidi Mehrabadi et al.[15] We categorize these two groups as highly aggressive and secondarily aggressive. Secondly, we examine the expression of *Pcna*, which is a well-recognized marker of cellular proliferation.[25] We found that cellular proliferation *in vitro* is the lowest in the highly aggressive sublines and highest in the secondarily aggressive sublines. Since tumor growth *in vivo* is determined by the counteraction between proliferation and immunogenicity of cancer cells,[26] we expect that the less aggressive, more highly proliferative phenotype (e.g., subline C1) is more immunogenic and therefore more likely to respond to ICB treatment. By contrast, the more aggressive, less proliferative phenotype (e.g., subline C11) suggests lower immunogenicity and resistance to ICB treatment. Indeed, in preclinical studies where tumors of sublines C1, C11, C14, and C15 underwent anti-CTLA4 treatment, tumors of C1 and C14 were sensitive to treatment, with C1 showing markedly higher sensitivity than those of C14, and tumors of C11 and C15 were resistant.[24] Based on the observed phenotypes (growth rate, *Pcna* expression, and preclinical treatment studies on a subset of the sublines) and the putative treatment sensitivity implied by these phenotypes, we call the sublines C11, C15, C16, and C18 highly aggressive and resistant (HA-R) and sublines C1, C4, and C22 secondarily aggressive and sensitive (SA-S). We test for adaptation of gene expression in these two subline groups in order to identify genes with expression associated with the differences in phenotypes. As a control, we also test for adaptation within sublines C3, C10, and C14, which show mixed aggression, varying expression of *Pcna*, and C14 was shown to be sensitive to anti-CTLA4 treatment. We call this group mixed aggression and sensitive (MA-S).

Model

To understand how gene expression in different sublines shifts due to selective pressures, we use stochastic models to estimate such shifts for each of the phenotypically distinct groups of sublines. Finding genes that adapt differently between the sublines will give insight into how the sublines have adapted to exhibit contrasting growth rates and resistance to ICB therapies.

Our approach to modeling clonal gene expression evolution builds upon OU processes that are often used to study the evolution of gene expression across species.[17,20–22,27,28] Instead of species, we apply our method to the sublines evolved from a cell of common origin. We assume that the evolution of gene expression in a tumor is a stochastic process that follows one of three alternative evolutionary models: neutral (no selection), constrained (putative negative selection), or adaptive (expression shift consistent with clone(s) adaptation) evolution. Neutral evolution is expected to occur when there are no selective pressures on the expression. We model neutral evolution with a Brownian motion (BM) process, where changes to gene expression occur randomly at each time step (Figure 3A; box 1). Constrained evolution is expected when there is a selective pressure against a divergence from a common optimal value acting on all sublines. We model constrained evolution with an OU process with a single optimum: the gene expression for all sublines converges toward a common value, θ_0 (Figure 3A; box 2). Adaptive evolution is expected to occur when selective pressures cause the sublines to adapt (shift expression) to different values (Figure 3A; box 3). We model adaptive evolution as an OU process with two optima,[3] θ_0 and θ_1. In order to evaluate adaptive evolution,

the sublines must be partitioned into groups expected to have different optima values; this partitioning is called a "regime." In this setting, one set of the sublines is the group of interest, hereafter called the "chosen" sublines, and the rest of the sublines are considered as "background." In species evolution, such adaptation might be a result of differing environments. For example, fruit flies have shown adaptation of gene expression based on feeding patterns, which could result from selective pressures based on the type of food available.[17] In clonal evolution, selective pressures would come from the tumor microenvironment. The selective pressures of the microenvironment could vary across different cells, for example, because of their location within the tumor. Adaptation can also occur when there is a single selective pressure, but the species/cells change in different ways to fill different niches in the environment. For example, cells may develop different methods for escaping immune response. Further details of BM and OU processes can be found in the STAR Methods.

To detect constrained and adaptive evolution of gene expression from single-cell RNA sequence data of the sublines, we use EvoGeneX, a recently introduced software.[17] EvoGeneX takes as input the phylogenetic tree, the expression data for the gene under evaluation, and the regime for the adaptive evolution model; it outputs whether the gene can be considered to be constrained or adaptive. We evaluate three regimes of interest based on the groups of sublines sharing phenotypic properties described above: highly aggressive and resistant (HA-R), secondarily aggressive and sensitive (SA-S), and mixed aggression and sensitive (MA-S). The internal nodes are assigned optima based on the shared ancestry of the phylogeny built from bWES data[15] of the chosen sublines in that regime (Figure 2B). We run EvoGeneX on each regime independently. For each regime, all sublines not in the group under evaluation are used as the background for comparison.

EvoGeneX detects adaptation for each gene as follows. First, it uses maximum likelihood to estimate the model parameters and calculate a likelihood value for each of the three models (BM, OU with one optimum, and OU with two optima). The stochastic processes are computed down the branches of the tree, with the number of steps of each process proportional to the branch lengths, and lineages sharing internal branches sharing the same values. Second, it calculates a p value by using likelihood ratio tests to determine if neutral evolution can be rejected for constrained or adaptive evolution. After running EvoGeneX for all genes, we calculate q values by correcting the p values for multiple hypothesis testing using the Benjamini-Hochberg false discovery rate (BH-FDR) method. Genes are labeled as constrained or adaptive if the q value from the likelihood ratio test against neutral evolution is less than 0.05.

Because EvoGeneX estimates the parameter values of each model, the adaptive genes can be considered to be adaptively upregulated or adaptively downregulated by comparing the estimated optima values of the chosen sublines in the regime of interest and the background: if the chosen sublines have a higher estimated optimum than the background, the genes are considered to be adaptively upregulated, and if they have a lower estimated optimum, they are considered to be adaptively downregulated.

EvoGeneX utilizes biological replicates to estimate within-species expression variability. The use of replicates is vital when using OU processes to reduce false positive results.[17,22,29] In the case of species, the biological replicates are different individuals of the same species. In our setting, the individual cells sequenced for each subline serve as these biological replicates. Accounting for such within-subline variation decreases potential false positives that could result from high variation within each subline as well as from the noise inherent in single-cell data.

Applicability of the OU-based model for single-cell cancer data and validation with simulations

Previous studies inferring gene expression evolution of species with OU models utilized bulk data from tissues, organs, or even whole organisms.[17,18,28] However, bulk data represent the average expression across all the cell types in the population. Because of this aggregation, when the composition of the cellular population changes, the bulk expression value also changes. Such settings do not allow for differentiating expression shift driven by evolution within specific cell types from shift driven by evolution of tissue composition.[29] Distinguishing evolutionary changes from compositional changes is particularly relevant in the context of cancer, where subclonal growth and selection change the cellular composition of the tumor. However, single-cell data come with unique challenges, especially high noise. To confirm that OU-based modeling is effective for such data, we perform simulation studies.

In our simulation studies, we generated expression data using an OU process on the evolutionary tree inferred for our data (Figure 2B)[15] under different modes of evolution. Adaptive evolution was simulated under the HA-R regime. For the constrained and adaptive simulations, we varied the parameters to reflect both strong and weak signals of adaptation. We added varying levels of noise to reflect the nature of single-cell measurements, aiming to obtain similar expression patterns as in the experimental data. To do this, we simulate replicates as being pulled from a negative binomial distribution. The negative binomial distribution includes a parameter to tune the within-species variation, increasing the noise to be similar to single-cell data (details on simulated data generation can be found in the STAR Methods). We then evaluated whether our approach using EvoGeneX could correctly infer the evolutionary model used to generate the data. Our simulation studies confirmed that in this setting EvoGeneX can uncover expression adaptation, with the accuracy depending on the model parameters: the distance between the optima, the pull toward the optima, and the within- and between-subclone variation. Depending on these parameters, EvoGeneX correctly identified up to 95% of genes simulated to have adaptive expression as adaptive (identifying 42% across all parameter combinations). It also had a low false positive rate: of all neutrally evolving experiments, a total of only 3.4% genes were predicted to be adaptive (Figure 3B). However, in this setting, EvoGeneX could not reliably distinguish constrained evolution from neutral evolution. Thus, in the remainder of the paper, we focus on inferring adaptation only.

Finally, we used the simulation study to test if OU-based models provide an advantage over differential expression analysis as a basis to infer adaptation. We performed differential expression (using an independent t test on the simulated expression data with Benjamini-Hochberg FDR corrected q value $<$ 0.05.) between the genes simulated in the chosen sublines and

background sublines. In real data, the groups are unknown, and clustering methods are used to identify them. We use the known divisions rather than a clustering step to better compare differential expression analysis and EvoGeneX.

More adaptive genes were detected to be differentially expressed than were identified by EvoGeneX to be adaptive (across all simulations 46% of genes are differentially expressed compared with 42% being predicted as adaptive by EvoGeneX), though the difference is not statistically significant (Figure 3B). However, differential expression had a much higher false positive rate of adaptive predictions: 26.3% of neutrally simulated genes were identified as differentially expressed compared with 3.4% identified as adaptive by EvoGeneX (statistically significant [$p < 0.01$]; Figure 3B). Although differential expression can sometimes identify more adaptive genes than are predicted by EvoGeneX, the high false positive rate demonstrates that our method using EvoGeneX is applicable to single-cell RNA sequence data and is more useful for identifying potential adaptation in this setting than differential expression analysis alone. Details of how each simulation parameter influences the results of EvoGeneX and differential expression can be found in Figures S1 and S2.

Gene expression adaptivity is distinctly contrastive in subclones with different phenotypes

Given the distinct subclonal phenotypes observed, our goal was to identify genes with expression under adaptive evolution driving the properties of the HA-R and SA-S subline groups. To address this question, we used EvoGeneX to identify genes with expression patterns consistent with adaptive evolution for each regime as described in the previous section. We also evaluate the MA-S subline group as a control to tell how many genes could have adaptive expression when sharing ancestry but not phenotype.

The single-cell RNA sequencing captured 55,401 genes that were measured in at least one cell.[15] We used only the 8,363 genes that had at least one non-zero expression value for every subline. Of these 8,363 genes analyzed, we identified 812 (9.7%) genes with adaptive expression in HA-R (496 adaptively upregulated and 316 adaptively downregulated), 1,277 (15.3%) genes with adaptive expression in SA-S (201 adaptively upregulated and 1,076 adaptively downregulated), and 616 (7.4%) genes with adaptive expression in MA-S (288 adaptively upregulated and 328 adaptively downregulated). Full results are reported in Tables S1–S3. Consistent with our simulation studies, we found no constrained genes. As expected, there are more genes with adaptive expression predicted in the HA-R and SA-S subline groups that share phenotypes than in MA-S, which has mixed phenotypes. We further confirm that the genes with adaptive expression identified in HA-R and SA-S are not due to noise, by running EvoGeneX over randomly selected subline groups. We found that random groups generally result in fewer genes with adaptive expression than HA-R and SA-S and about the same number as MA-S (Figure S3). Additionally, we compare the results of clustering the sublines based on the expression of all the genes or only the genes with adaptive expression in at least one chosen subline group. We find that using the genes with adaptive expression results in better clustering of sublines with shared phenotypes (Figure S4).

We performed enrichment analysis on KEGG pathway database to investigate the functions of the genes with adaptive expression in each regime. Because we expect that the genes with adaptively upregulated and adaptively downregulated expression will have different functions, we run enrichment analysis on them separately. The genes with adaptively downregulated expression in HA-R and adaptively upregulated expression in SA-S are enriched for "ribosome."[4] Ribosomal pathways are involved in cell growth, so this contrasting enrichment is consistent with the phenotypes of the sublines. The genes with adaptively downregulated expression in SA-S are enriched for "Rap1 signaling pathway" and "bacterial invasion of epithelial cells." Upregulation of Rap1 signaling pathway has been shown to be associated with cellular migration,[30] which was not observed in SA-S but was in HA-R (see section "functional implications of genes with adaptive expression patterns in melanoma"), again showing consistency with the subline phenotypes. The genes with adaptively upregulated expression in MA-S are enriched for "pathways of neurodegeneration." The genes in pathways of neurodegeneration are mostly mitochondrial and related genes. There is no significant enrichment for KEGG pathways for the genes with adaptively upregulated expression in HA-R or adaptively downregulated expression in MA-S. The pathway enrichment for each regime is shown in Figure 4A, and the specific genes involved in each enrichment are listed in Table S4.

We performed k-means clustering on the genes with adaptive gene expression in at least one of the regimes (see STAR Methods for details) and present the results in a heatmap (Figure 4B; Table S5). As can be seen, there are large clusters of genes that are largely only adaptive in one regime (e.g., clusters 0, 3, and 6), but there is also distinct overlap between the regimes. For example, genes in clusters 1 and 2 have adaptively upregulated expression in HA-R but adaptively downregulated expression in SA-S, while genes in clusters 7 and 8 have the opposite adaptive expression pattern between these two regimes. In parallel, genes in clusters 1 and 4 have adaptively upregulated expression in MA-S but adaptively downregulated expression in SA-S.

We then investigated how the genes associated with enriched pathways were distributed across clusters. Clusters 1, 2, and 3, which are composed of genes with adaptively downregulated expression in SA-S, contain the genes that are in the enriched pathways "Rap1 signaling" and "bacterial invasion of epithelial cells." Many of these genes also have adaptively upregulated expression in HA-R (clusters 1 and 2). By contrast, clusters 7, 8, and 9, which are composed of genes with adaptively upregulated expression in SA-S, contain the genes that are in the enriched "ribosome" pathway, and many also have adaptively downregulated expression in the HA-R sublines (clusters 7 and 8). Together, these results suggest that the sublines with contrasting phenotypes evolved to have distinct transcriptional states.

Functional implications of genes with adaptive expression patterns in melanoma

In this section, we provide more detailed biological interpretation of the adaptivity profiles between the sublines. Specifically, we analyze the genes within the clusters with adaptively upregulated expression in the HA-R and SA-S subline groups.

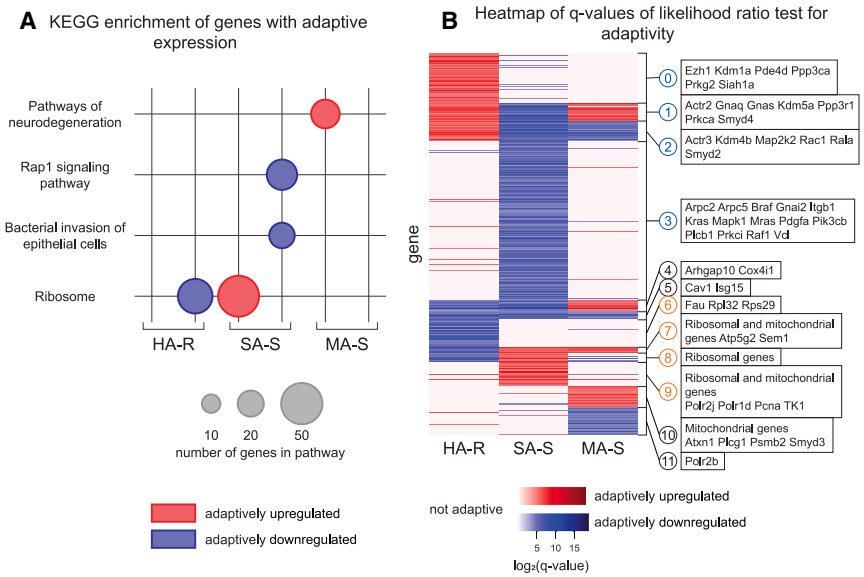

Figure 4. Pathway enrichment and clustering analysis of genes with adaptive expression

(A) KEGG enrichment of genes with adaptive expression. Enrichment analysis was performed on the genes with adaptively upregulated and adaptively downregulated expression in each regime separately. Pathways with a q value (Benjamini-Hochberg false discovery rate corrected p value) less than 0.05 were considered significant. For each subline group, enrichment results for genes with adaptively upregulated expression for each subline group are shown in red on the left, and results for genes with adaptively downregulated expression are shown in blue on the right. The size of the dot represents the number of genes present in that enriched pathway.

(B) Heatmap of genes with adaptive expression, grouped into 12 clusters, and example genes in each cluster. Each row is a gene that has adaptive expression in at least one of the subline groups. Colors are based on the log of the q value for each gene, with adaptively upregulated expression shown in red and adaptively downregulated expression shown in blue. Genes with expression that are not adaptive in a subline group are shown in white. Clusters labeled in blue have adaptively upregulated expression in the HA-R and/or adaptively downregulated expression in the SA-S sublines (but not adaptively downregulated expression in both). Clusters labeled in orange have adaptively upregulated expression in the SA-S sublines and/or adaptively downregulated expression in the HA-R sublines (but not adaptively downregulated expression in both). See the STAR Methods for clustering methods.

We first consider the genes with adaptively upregulated expression in HA-R (clusters 0, 1, and 2). We found many genes involved in G protein-coupled receptor (GPCR) signaling and cell invasion. They include G protein signaling (*Gnaq*, *Gnas*, and *Rab5b*), their direct downstream effectors such as phosphodiesterases (*Pde10a* and *Pde4d*), protein kinase G (PKG) (*Prkg2*), protein kinase C (PKC) (*Prkca*), and the further downstream calcineurin genes (*Ppp3r1* and *Ppp3ca*). These suggest their involvement in GPCR signaling, which regulates cell invasion, mesenchymal transition, formation of polarity, etc. In these clusters, we also find cytoskeleton and cell adhesion-associated proteins (*Actr2*, *Actr3*, *Arhgef2*, *Arhgap17*, etc.) and membrane receptor downstream effectors (*Rac1*, *Map2k2*, etc.). These genes are relevant to the function of cell migration, adhesion, and survival. Many of the genes included in the enrichment for the Rap1 signaling pathway and bacterial invasion of epithelial cells in the SA-S sublines also have adaptively upregulated expression in HA-R (e.g., *Gnaq*, *Gnas*, *Prkca*, *Actr2*, and *Actr3*). Both of these pathways are involved in tumor cell migration, invasion, and metastasis, and have many genes shared with the non-canonical Wnt signaling pathway,[31] which has been known to drive the "invasive" phenotype of melanoma.[32]

Next, we examined the genes with adaptively upregulated expression in SA-S (clusters 7, 8, and 9). In addition to the enrichment in ribosomal genes uncovered by KEGG analysis, we also find mitochondrial-related genes in these clusters, including *Atp5g2* and *Sem1*. Ribosomal and mitochondrial genes are upregulated in MITF-high (proliferative) melanoma,[33] which is associated with the canonical Wnt signaling pathway.[32] Since these genes are important for cellular growth, we also examined other genes with adaptive expression in SA-S and found that cellular growth genes, including nucleotide metabolism gene *Tk1*, RNA polimerase subunits (*Polr2j* and *Polr1d*), and cell cycle gene (*Pcna*), have adaptively upregulated expression in these sublines.

The KEGG enrichment analysis and the functional analysis of genes with adaptive expression jointly suggest that the HA-R and SA-S sublines are related to the classic invasive and "proliferative" phenotypes of melanoma, respectively. Developmentally, the former is associated with a more undifferentiated, mesenchymal state, and the latter with a differentiated, melanocytic state.[34] During tumor growth, the proliferative subtype has advantages over the invasive subtype. However, under the therapy-induced stress, the invasive subtype gains advantages over the proliferative subtype.[35] It has been proposed that these two phenotypes of melanoma are controlled by two distinct Wnt[5] pathways. The proliferative phenotype is controlled by the canonical Wnt pathway, which is mediated through β -catenin to activate *Mitf* expression, resulting in the induction of genes for cell growth and proliferation.[32,33] The invasive melanoma phenotype is controlled by non-canonical Wnt signaling, which activates PKC/Ca^{2+} signaling to promote cell migration and invasion.

Therefore, we examined if the genes with adaptive expression are involved in the Wnt signaling pathways in a subline-group-dependent way. As summarized in Figure 5, proliferation-associated genes in clusters 7 to 9, where the SA-S sublines have adaptively upregulated expression (e.g., ribosomal and mitochondrial genes; cell cycle and RNA polymerase genes) are involved in the canonical Wnt signaling pathway. By contrast, invasion-associated genes in clusters 0, 1, and 2, where the HA-R sublines have adaptively upregulated expression (e.g., G protein subunits, phospholipase C [PLC] genes, protein kinase C [PKC] genes, protein kinase G [PKG] genes, calcineurin genes, and actin remodeling genes), are involved in the non-canonical Wnt signaling.

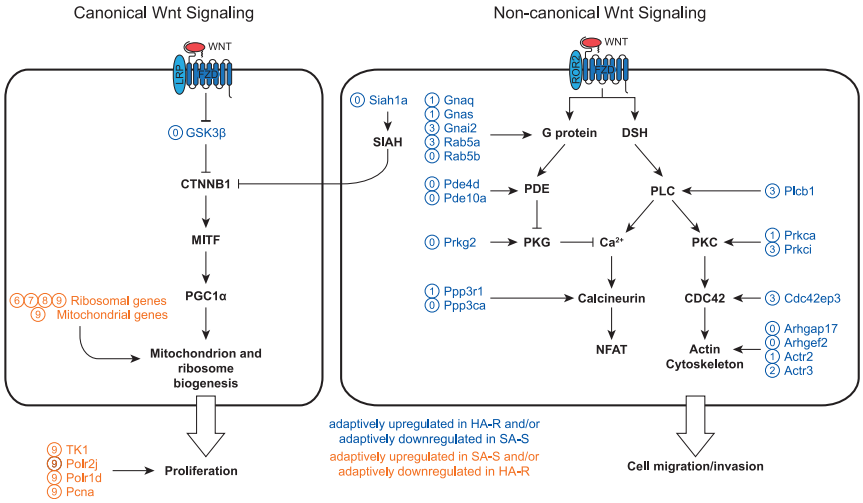

Figure 5. Adaptively expressed genes associated with WNT signaling in melanoma

The effectors and signal transduction in each pathway are shown in bold black font. The genes are labeled with the cluster they belong to in the heatmap of Figure 4B and colored consistently: genes in blue have adaptively upregulated expression in HA-R and/or adaptively downregulated expression in SA-S (but not adaptively downregulated expression in both), and genes in orange have adaptively upregulated expression in SA-S and/or adaptively downregulated expression in HA-R (but not adaptively downregulated expression in both).

(Left) Canonical WNT signaling. The WNT ligand (e.g., *WNT1* and *WNT3A*) binds to the composite receptor, *LRP* and frizzled (*FZD*), resulting in the inhibition of *GSK3*β and activation of β -catenine (*CTNNB1*). *CTNNB1* activates *MITF*, which induces the expression of *PGC1*α, ribosomal genes, and melanocytic differentiation genes such as *DCT*, tyrosinase (*TYR*), *TRP1*, etc. *PGC1*α drives the biogenesis of mitochondria. The overall effect is to promote cell differentiation, growth, and proliferation.

(Right) Non-canonical WNT signaling. The WNT ligand (e.g., *WNT5A* and *WNT11B*) binds to the composite receptor, *ROR* and *FZD*, resulting in the activation of calcium signaling through G proteins, phosphodiesterase (PDE), and protein kinase G (PKG), or through disheveled (DSH) and phospholipase C (PLC). The released calcium (Ca^{2+}) will bind to and activate calcineurin, resulting in the activation of NFAT, a transcription factor that control cellular differentiation.[36] The PLC signaling may also activate protein kinase C (PKC), which in turn promotes cell migration and invasion though *CDC42* and cytoskeleton reorganizing genes. The overall effect is to promote epithelial-mesenchymal transition (EMT), cell migration, and invasion.

We also found histone modification enzyme genes with adaptively upregulated expression in HA-R and adaptively downregulated expression/no selection in SA-S, including *Kdm1a*, *Ezh1* (cluster 0), *Kdm5a*, *Smyd4* (cluster 1), *Kdm4b*, *Smyd2* (cluster 2), and *Smyd3* (cluster 10). Since histone modification can determine the activation or inactivation of transcription,[37] these genes may serve as a "switch" of specific gene modules and therefore have expression undergoing selection. In fact, Siah and Kdm genes have been shown to switch cells from canonical to non-canonical WNT signaling.[38] *Gsk3*β, which has adaptively upregulated expression in HA-R, can also act as a switch between the two signaling pathways by inhibiting canonical Wnt signaling (Figure 5, left panel).

In summary, the genes with adaptively upregulated expression in the HA-R sublines are associated with cell invasion and non-canonical Wnt signaling. By contrast, the genes with adaptively upregulated expression in the SA-S sublines are associated with cell proliferation and canonical Wnt signaling. Taken together, these results imply that gene modules controlling specific functions and transcriptional states of the cells are subject to selection during melanoma subclonal evolution.

Genes with adaptively evolving expression underline therapeutic responses

In the above analysis, we identified genes with adaptive expression in two different groups of sublines that represent subclones displaying contrasting phenotypes. Presumably, the expression of these genes was selected for by the tumor microenvironment, such as immune response and competition for nutrients. These selective pressures gave rise to the distinct phenotypes of the sublines, particularly *in vivo* growth rate and response to immunity, in a process of adaptation.

However, the 23 sublines isolated and analyzed in these experiments are expected to be only a small sample of all subclones present in the parental line B2905. We validate that our results are representative of other subclones that display similar phenotypes as the analyzed sublines. Specifically, we analyzed genes differentially expressed in B2905-derived tumors sensitive and resistant to ICB treatment and examined how they are associated with genes exhibiting adaptive expression based on our evolutionary analysis of the sublines.

The response of tumors derived from the parental B2905 cell line to ICB treatment was determined in a preclinical study described previously.[39] Briefly, mice bearing tumors grown from implanted parental B2905 cells were subjected to anti-CTLA4 or isotype control immunoglobulin G (IgG) treatment. After the completion of the dosing, tumors that continuously increased or decreased/remained stable in size for a pre-defined period of time were identified as non-responder and responder tumors, respectively (Figure 6B), and harvested for bulk RNA sequencing. We use a total of 25 mice (14 responders, 6 non-responders, and 5 control).

Tumors that effectively respond to ICB treatment are expected to exhibit higher levels of therapy-induced immunity, reducing the cellular population to resistant subclones after treatment (Figure 6A). To test if the post-treatment responder tumors are indeed dominated by resistant subclones, we evaluated the melanocytic plasticity signature (MPS) score and CD8 expression of the treated tumors (Figure 6C). A high MPS score indicates higher undifferentiated state that is associated with resistance to immunotherapy[23] and has been used in previous studies to examine treatment resistance.[15] The CD8 score (the average of *CD8a* and *CD8b* gene expression) has been used to quantify the infiltration of effector T cells into tumors, indicating the degree of inflammatory responses.[40] As compared with the post-treatment non-responder tumors, the responder tumors have significantly higher MPS scores (independent t test p value < 0.001) as well as higher (though not significant) CD8 scores, suggesting

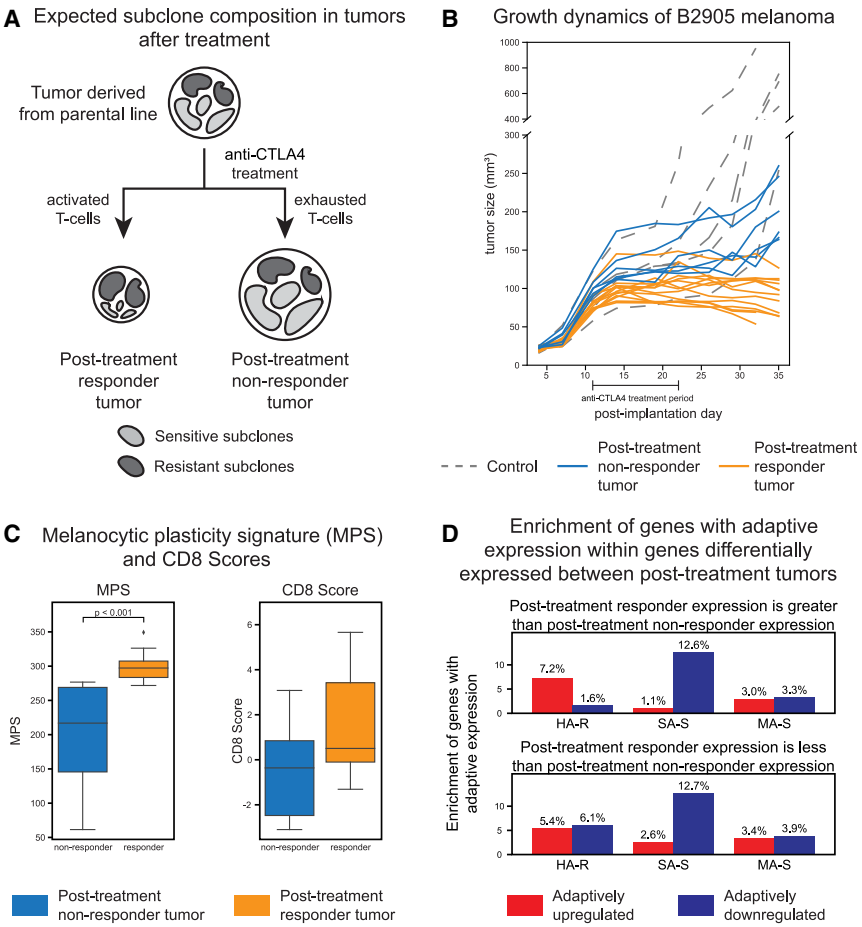

Figure 6. Adaptively upregulated genes of HA-R were selected by therapy-induced immunity in a preclincial study

(A) The hypothesis of subclonal responses to immunotherapy in melanoma. Parental tumors that contain all subclones are treated with anti-CTLA4. The therapy could induce effective immunity, resulting in tumor response by reducing the size of the sensitive subclones (light gray) and selecting resistant subclones (dark gray), or fail to induce effective immunity, which results in no response and growth of all subclones.

(B) Growth of 5 tumors under IgG2b (control; dashed gray lines) and 20 tumors under anti-CTLA4 treatment (orange and blue lines). The x axis is the day after implantation, and the y axis is the size of the tumor in mm^3. Four doses were given in the period of days 11–22 (bar under x axis). The anti-CTLA4-treated tumors can be divided into 14 responders, where the tumor stopped growing (orange), and 6 non-responders, where the tumor continued to grow (blue).

(C) The MPS (left) and CD8 (right) scores of the post-treatment 14 responder and 6 non-responder tumors (see text). *p* value shown is from an independent t test between the two groups.

(D) The enrichment of genes with adaptive expression in the genes that are differentially expressed between post-treatment responder and non-responder tumors. The top plot shows genes with higher expression in the post-treatment responder tumors, and the bottom plot shows genes with higher expression in the non-responder tumors. The y axis shows the percentage of the differentially expressed genes that have adaptive expression. The x axis shows the different groups of sublines. Each subline group is separated into genes with adaptively upregulated (red, left) and adaptively downregulated expression (blue, right).

therapy-induced effective inflammatory response. This confirms that effective immune response reduces the responder tumors to more undifferentiated, resistant subclones.

The resistant subclones that persist after immune treatment are likely to include a broader set of subclones than just those isolated for the single-cell analysis. This provides an opportunity for testing whether genes identified as having adaptive expression using the representative set of sublines are more broadly related to immunotherapy response. If the identified adaptivity is characteristic of immunotherapy response, then the post-treatment responder tumors should be enriched in genes with adaptive expression in the HA-R sublines because of the dominance of resistant subclones in those tumors. Specifically, when a gene has high expression in the post-treatment responder tumors, that gene is expected to have adaptively upregulated expression in HA-R sublines, and when a gene has low expression in the responder tumors, that gene is expected to have adaptively downregulated expression in HA-R sublines.

To investigate the enrichment of genes with adaptive expression in the clonal sublines, we first performed differentially expressed gene (DEG) analysis between post-treatment responder and non-responder tumors using DESeq2.[41] Of the 2,268 DEGs that are also in the single-cell dataset used to test for adaptivity, 642 and 1,626 have higher relative mean expression in the post-treatment responder and non-responder tumors, respectively. Full results are reported in Table S6.

We then examined the enrichment of genes with adaptive expression within the DEGs by calculating the percentage of adaptively expressed genes in the DEGs (Figure 5D). As expected, the DEGs that are more highly expressed in the post-treatment responder tumors are preferentially enriched with genes with adaptively upregulated expression in the HA-R sublines relative to those with adaptively downregulated expression (7.2% versus 1.6%). By contrast, DEGs more highly expressed in post-treatment non-responder tumors are preferentially enriched with genes with adaptively downregulated expression in the HA-R sublines relative to those with adaptively upregulated expression (6.1% versus 5.4%), although this trend is less distinct. The differences between these enrichment patterns are statistically significant (chi-squared p value < 0.0001). These patterns demonstrate that the genes identified as having adaptive expression in the HA-R sublines are indeed more highly expressed in the post-treatment responder tumors that experienced effective treatment and represent a resistant population of cells not restricted to the tested sublines.

Next, we analyzed the genes with adaptive expression in the SA-S sublines. The DEGs with higher expression in the post-treatment responder tumors are preferentially enriched with

genes with adaptively downregulated expression relative to those with adaptively upregulated expression (12.6% versus 1.1%). The genes with higher expression in the post-treatment non-responder tumors also have higher enrichment with genes with adaptively downregulated expression relative genes with adaptively upregulated expression (12.7% versus 2.6%). This trend may be because of the likely heterogeneity of the post-treatment non-responder tumors (Figure 5A). These enrichment differences are statistically significant (chi-squared p value < 0.05). Genes with adaptive expression in the MA-S sublines do not show significant preferential enrichment. This suggests that the enrichment shown by HA-R and SA-S is associated with their phenotypes.

These analyses further support the view that genes identified to have adaptively upregulated expression in HA-R are broadly related to the invasive and ICB-resistant tumor phenotype. Notably, signaling that drives melanoma cells toward invasive/migratory/epithelial-mesenchymal transition (EMT) phenotype similar to HA-R has been shown to associate with resistance to immunotherapies.[34,42]

DISCUSSION

Summary

In this study, we utilized BM and OU processes to model adaptive evolution of gene expression in mouse melanoma tumors. By running our method on clonal sublines derived from a mouse melanoma model exhibiting distinct phenotypic properties, we were able to identify genes with adaptive expression within groups of sublines. Specifically, we focused on sublines that varied in their growth rate and response to anti-CTLA4 immunotherapy treatment when implanted individually into distinct but genetically identical mice.

We found that about 9%–15% of the genes have expression that can be considered to be adaptive within the subline groups sharing phenotypes. The genes with adaptive expression in sublines that were highly aggressive and resistant to ICB therapy (HA-R) are associated with cell invasion, cell migration, adhesion, and survival. By contrast, the genes with adaptive expression in the sublines that were secondarily aggressive and sensitive to ICB therapy (SA-S) are associated with ribosomal and mitochondrial processes, indicating cell growth. These two groups of genes represent the known binary invasive and proliferative phenotypes of melanoma. Additionally, the genes with adaptively upregulated expression in the HA-R sublines are associated with non-canonical Wnt signaling, while the genes with adaptively upregulated expression in the SA-S sublines are associated with canonical Wnt signaling, further supporting the link with the binary phenotypes in melanoma.[34]

We also evaluated the genes with adaptive expression in tumors derived from the parental line and treated with anti-CTLA4 immunotherapy. We found that tumors with therapy-induced immunity were enriched with genes with adaptive expression in HA-R. This is consistent with a previous study showing that resistance of melanoma to ICB is associated with the precursor states.[23] Our results suggest that genes in functional modules are subjected to selection together. Such gene modules are usually involved in the developmental process.[43] For example, we identify selection on gene expression related to non-canonical and canonical Wnt signaling genes. These genes are involved in the migration and maturation phase of melanocyte precursors.[44] Our findings also indicate that selection of gene modules could be achieved by the adaptively upregulated expression of histone modification enzyme genes, which can serve as genetic switches of gene groups.

Stochastic models of gene expression expand on traditional mutation- and sequence-based methods

In contrast to previous tumor evolution analyses that focus on mutations, our analysis focuses on the evolution of gene expression. The insights from expression-based evolutionary analysis using a mutation-based phylogeny are complementary to analyses using mutations alone. In particular, we found that mutated genes are not more likely to have adaptive expression: the percentage of mutated genes that have adaptive expression is nearly equal to the percentage of all analyzed genes that have adaptive expression. This suggests that our results would not be identifiable if solely using mutations. This may imply the distinct roles of genetic and non-genetic drivers of subclonal evolution. In addition, we performed analysis with traditional dN/dS methods, which are used to determine adaptivity in the context of sequence evolution. dN/dS analysis across the entire genome and all sublines found a signal consistent with weak positive selection (1.63). Performing dN/dS on the chosen subline groups separately, we also mostly found signal consistent with weak positive selection (1.32, 1.80, and 1.46 for HA-R, SA-S, and MA-S, respectively). This is consistent with previous studies that found slight positive selection in cancer tumors.[45] However, the sparsity of mutational data did not allow for detailed gene-wise analysis. Details of the dN/dS analysis can be found in the STAR Methods. Thus, the modeling of gene expression evolution in cancer provides unique insights into tumor evolution that an analysis based on mutations alone would miss.

Limitations of the study

There are limitations of our study that open possibilities for future work. First, because of the noise in single-cell data, our method, like differential expression and sequence-based dN/dS methods, is unable to distinguish weak signals of constrained evolution from neutral evolution, as shown in our simulation studies. This makes it unsurprising that we do not identify any genes with constrained expression evolution in the biological data. However, we cannot rule out the possibility that tumors evolve with limited constrained evolution. This question could be further investigated by leveraging bulk RNA sequencing, which has less noise, in conjunction with single-cell data.

Second, when analyzing sublines from one regime (e.g., HA-R), the sublines in the other regimes (e.g., SA-S and MA-S) are considered as part of the background. Our results then must be considered comparatively. This could result in genes that are only in fact adaptively upregulated in one regime being also labeled as adaptively downregulated in the others. To help avoid comparative results, OU models allow for more than two optima to be estimated. In order to address whether using only two optima impacted our results, we ran experiments with such further divisions, considering the case where the HA-R, the SA-S, and the rest of the sublines all have separate optima. The results of this three-regime experiment were similar to the

two-regime results, giving us increased confidence that our results using two optima can be generalized. Using more optima increases the number of parameters to estimate and reduces the power of the stochastic methods, resulting in fewer genes being properly estimated. Designing new methods that can better optimize over additional optima would allow us to further support our results and enable future studies examining multiple groups of sublines.

Further, previous studies in species evolution have suggested that the size and branch length of the evolutionary tree can impact the results of BM and OU methods, where increasing the number of leaves and lengths of branches improved model performance.[17,22,46] While our tree has 23 leaves, more than other studies of species evolution,[17,21,28] it is possible that adding more sublines could provide even further insights.

Our model does not address the mechanisms altering the expression of the genes. Adaptation of gene expression can be mediated by many different mechanisms, including genetic, epigenetic, and metabolic alterations. Changes in these mechanisms may not impact the gene expression directly but rather promote indirect changes, like epistatic interactions. For example, we have shown that genes with adaptive expression in the HA-R sublines include epigenetic control genes, specifically histone modification enzymes (section "functional implications of genes with adaptive expression patterns in melanoma"). This result suggests epigenetic changes contribute to the evolution of gene expression. Independent of the regulatory mechanisms mediating the gene expression changes, adaptation of gene expression indicates regulation of activities of genes and pathways directly impacting phenotypes of interest such as growth, proliferation, and immunotherapy resistance. Information of gene expression adaptation provides a window for understanding selective forces in cancer evolution and can guide efficient approaches to therapy.

Despite these limitations, our method was able to identify genes with adaptive expression, and our subsequent analysis reveals that these adaptive genes were associated with specific pathways directly linked to the subline phenotype. We were unable to identify these genes from dN/dS analyses or mutations alone, demonstrating the benefits of gene expression evolution analyses for studying subclonal evolution and response to treatment. Examining adaptation of gene expression can be used in many further applications. For example, comparing gene expression adaptation between cancer types and patients of different sex and/or age can reveal further understanding of both general adaptation trends in cancer as well as differences based on specific microenvironments of individuals.

Conclusions

In conclusion, our study demonstrates the efficacy of using stochastic processes for modeling gene expression evolution of tumor sublines in the context of uncovering clone-specific adaptation. Applying our methodology to mouse melanoma sublines revealed adaptive evolution patterns consistent with the subline phenotype and response to treatment. Specifically, sublines that were resistant or sensitive to treatment had phenotype-specific profiles of genes with adaptive expression. This finding led us to discover pathways undergoing selection, specifically Wnt signaling, that vary between the sublines with contrasting phenotypes. Subsequent gene expression analysis of tumors grown from the parental line and subjected to anti-CTLA4 treatment showed that the genes identified to have adaptive expression based on our analysis of isolated sublines are broadly associated with the corresponding phenotype. Our methodology for analyzing clonal sublines identified phenotype-switching signaling that could not be revealed by mutations only.

Our results demonstrate that analysis of single-cell sequencing data using stochastic models can identify genes and functional modules with expression undergoing adaptation, which is key information in tumor evolution and heterogeneity. Knowledge of the functions of subclones selected by specific microenvironments can further allow for the design of effective treatment protocols.

RESOURCE AVAILABILITY

Lead contact

Further information and requests for resources and reagents should be directed to and will be fulfilled by the lead contact, Teresa M. Przytycka (przytyck@ncbi.nlm.nih.gov).

Materials availability

This study did not generate new materials.

Data and code availability

- Single-cell RNA-seq data from the 23 subline study have been deposited at GEO and are publicly available as of the date of publication. Accession number is GEO: GSE215963.
- Bulk RNA-seq data from the preclinical study have been deposited at GEO and are publicly available as of the date of publication. Accession number is GEO: GSE255484.
- All original code has been deposited at Github: https://github.com/ncbi/nongenomic-evolution-of-tumor-subclones and is publicly available at Zenodo: https://doi.org/10.5281/zenodo.14037979 of the date of publication.
- Any additional information required to reanalyze the data reported in this paper is available from the lead contact upon request.

ACKNOWLEDGMENTS

M.G.H. and T.M.P are supported by the NLM Intramural Research Program (LM200887). S.P. is supported by the NEI Intramural Research Program. F.R.M., S.M., C.G., E.P.-G., C.S., G.M., and C.-P.D. are supported by the NCI Intramural Research Program. The research of E.P.-G., G.M., and C.-P.D. is supported in part by the FLEX Synergy Award from the NCI Center for Cancer Research. E.P.-G. is supported by the Spanish Agencia Estatal de Investigación and Ministerio de Ciencia e Innovacion (PID2022-141113OA-I00) and a MRA Young Investigator Award (#1037420) by the Melanoma Research Alliance. E.K.M. is supported by the State of Maryland. Computational experiments were performed on the compute cluster for the Center for Bioinformatics and Computational Biology at the University of Maryland, College Park. This work utilized the computational resources of the NIH HPC Biowulf cluster (http://hpc.nih.gov). The authors thank Ms. Sung Chin and Ms. Cari Smith (Laboratory Animal Science Program, Frederick National Laboratory for Cancer Research) for performing mouse studies and Dr. Yongmei Zhao (CCR Sequencing Facility Bioinformatics Group, Frederick National Laboratory for Cancer Research) for assistance coordinating the bulk treatment data.

AUTHOR CONTRIBUTIONS

M.G.H., E.K.M., C.-P.D., and T.M.P. were involved in conceptualization of the project. M.G.H., C.-P.D., S.M., F.R.M., and E.P.-G. performed data curation. M.G.H., E.K.M., C.-P.D., and T.M.P. performed the investigation. C.G., A.S.,

and E.P.-G. created the *in vitro* and *in vivo* models. M.G.H., S.P., C.-P.D., and T.M.P. developed the methodology of the project. M.G.H., C.-P.D., and T.M.P. performed the formal analysis. M.G.H. and S.P. developed the software used in this project. M.G.H., S.P., and C.-P.D. performed validation of the computational models. M.G.H. and C.-P.D. created visualizations. G.M. provided the melanoma cell line B2905 and its 24 sublines. M.G.H., E.K.M., C.-P.D., and T.M.P. wrote the original draft of the manuscript. S.P., C.S., and G.M. reviewed and edited the manuscript. E.K.M. and T.M.P. supervised the computational analysis; C.-P.D. supervised the preclinical study. T.M.P. and G.M. acquired funding for the project.

DECLARATION OF INTERESTS

The authors declare no competing interests.

STAR★METHODS

Detailed methods are provided in the online version of this paper and include the following:

- KEY RESOURCES TABLE
- EXPERIMENTAL MODEL AND SUBJECT DETAILS
- METHOD DETAILS
  - Determining adaptive genes with Brownian motion and Ornstein-Uhlenbeck models
  - Simulation studies
  - Random control runs
  - Clustering of genes with adaptive expression
- QUANTIFICATION AND STATISTICAL ANALYSIS
  - Function and pathway enrichment analysis
  - Differential expression analysis
  - dN/dS calculations

SUPPLEMENTAL INFORMATION

Supplemental information can be found online at https://doi.org/10.1016/j.cels.2024.11.013.

Received: February 24, 2024
Revised: August 30, 2024
Accepted: November 18, 2024
Published: December 18, 2024

REFERENCES

1. Nowell, P.C. (1976). The clonal evolution of tumor cell populations. Science *194*, 23–28. https://doi.org/10.1126/science.959840.
2. Vendramin, R., Litchfield, K., and Swanton, C. (2021). Cancer evolution: Darwin and beyond. EMBO J. *40*, e108389. https://doi.org/10.15252/embj.2021108389.
3. Scott, J., and Marusyk, A. (2017). Somatic clonal evolution: a selection-centric perspective. Biochim. Biophys. Acta Rev. Cancer *1867*, 139–150. https://doi.org/10.1016/j.bbcan.2017.01.006.
4. Beerenwinkel, N., Schwarz, R.F., Gerstung, M., and Markowetz, F. (2015). Cancer evolution: mathematical models and computational inference. Syst. Biol. *64*, e1–e25. https://doi.org/10.1093/sysbio/syu081.
5. Williams, M.J., Sottoriva, A., and Graham, T.A. (2019). Measuring clonal evolution in cancer with genomics. Annu. Rev. Genomics Hum. Genet. *20*, 309–329. https://doi.org/10.1146/annurev-genom-083117-021712.
6. Caiado, F., Silva-Santos, B., and Norell, H. (2016). Intra-tumour heterogeneity – going beyond genetics. FEBS J. *283*, 2245–2258. https://doi.org/10.1111/febs.13705.
7. Yang, D., Jones, M.G., Naranjo, S., Rideout, W.M., Min, K.H.J., Ho, R., Wu, W., Replogle, J.M., Page, J.L., Quinn, J.J., et al. (2022). Lineage tracing reveals the phylodynamics, plasticity, and paths of tumor evolution. Cell *185*, 1905–1923.e25. https://doi.org/10.1016/j.cell.2022.04.015.
8. Liu, Y., Li, X.C., Rashidi Mehrabadi, F., Schäffer, A.A., Pratt, D., Crawford, D.R., Malikić, S., Molloy, E.K., Gopalan, V., Mount, S.M., et al. (2023). Single-cell methylation sequencing data reveal succinct metastatic migration histories and tumor progression models. Genome Res. *33*, 1089–1100. https://doi.org/10.1101/gr.277608.122.
9. Saelens, W., Cannoodt, R., Todorov, H., and Saeys, Y. (2019). A comparison of single-cell trajectory inference methods. Nat. Biotechnol. *37*, 547–554. https://doi.org/10.1038/s41587-019-0071-9.
10. La Manno, G., Soldatov, R., Zeisel, A., Braun, E., Hochgerner, H., Petukhov, V., Lidschreiber, K., Kastriti, M.E., Lönnerberg, P., Furlan, A., et al. (2018). Rna velocity of single cells. Nature *560*, 494–498. https://doi.org/10.1038/s41586-018-0414-6.
11. Matsumoto, H., and Kiryu, H. (2016). Scoup: a probabilistic model based on the ornstein-uhlenbeck process to analyze single-cell expression data during differentiation. BMC Bioinformatics *17*, 232. https://doi.org/10.1186/s12859-016-1109-3.
12. Wang, L., Fan, J., Francis, J.M., Georghiou, G., Hergert, S., Li, S., Gambe, R., Zhou, C.W., Yang, C., Xiao, S., et al. (2017). Integrated single-cell genetic and transcriptional analysis suggests novel drivers of chronic lymphocytic leukemia. Genome Res. *27*, 1300–1311. https://doi.org/10.1101/gr.217331.116.
13. McCarthy, D.J., Rostom, R., Huang, Y., Kunz, D.J., Danecek, P., Bonder, M.J., Hagai, T., Lyu, R.; HipSci Consortium, and Wang, W. (2020). Cardelino: computational integration of somatic clonal substructure and single-cell transcriptomes. Nat. Methods *17*, 414–421. https://doi.org/10.1038/s41592-020-0766-3.
14. Shafighi, S.D., Kiełbasa, S.M., Sepúlveda-Yáñez, J., Monajemi, R., Cats, D., Mei, H., Menafra, R., Kloet, S., Veelken, H., van Bergen, C.A.M., et al. (2021). Cactus: integrating clonal architecture with genomic clustering and transcriptome profiling of single tumor cells. Genome Med. *13*, 45. https://doi.org/10.1186/s13073-021-00842-w.
15. Rashidi Mehrabadi, F., Marie, K.L., Pérez-Guijarro, E., Malikić, S., Azer, E.S., Yang, H.H., Kızılkale, C., Gruen, C., Robinson, W., Liu, H., et al. (2021). Profiles of expressed mutations in single cells reveal subclonal expansion patterns and therapeutic impact of intratumor heterogeneity. Preprint at bioRxiv. https://doi.org/10.1101/2021.03.26.437185.
16. Bastide, P., Soneson, C., Stern, D.B., Lespinet, O., and Gallopin, M. (2023). A phylogenetic framework to simulate synthetic interspecies rna-seq data. Mol. Biol. Evol. *40*, msac269. https://doi.org/10.1093/molbev/msac269.
17. Pal, S., Oliver, B., and Przytycka, T.M. (2023). Stochastic modeling of gene expression evolution uncovers tissue- and sex-specific properties of expression evolution in the drosophila genus. J. Comput. Biol. *30*, 21–40. https://doi.org/10.1089/cmb.2022.0121.
18. Bedford, T., and Hartl, D.L. (2009). Optimization of gene expression by natural selection. Proc. Natl. Acad. Sci. USA *106*, 1133–1138. https://doi.org/10.1073/pnas.0812009106.
19. Bertram, J., Fulton, B., Tourigny, J.P., Peña-Garcia, Y., Moyle, L.C., and Hahn, M.W. (2023). Cagee: computational analysis of gene expression evolution. Mol. Biol. Evol. *40*, msad106. https://doi.org/10.1093/molbev/msad106.
20. Butler, M.A., and King, A.A. (2004). Phylogenetic comparative analysis: a modeling approach for adaptive evolution. Am. Nat. *164*, 683–695. https://doi.org/10.1086/426002.
21. Brawand, D., Soumillon, M., Necsulea, A., Julien, P., Csárdi, G., Harrigan, P., Weier, M., Liechti, A., Aximu-Petri, A., Kircher, M., et al. (2011). The evolution of gene expression levels in mammalian organs. Nature *478*, 343–348. https://doi.org/10.1038/nature10532.
22. Rohlfs, R.V., Harrigan, P., and Nielsen, R. (2014). Modeling gene expression evolution with an extended ornstein-uhlenbeck process accounting for within-species variation. Mol. Biol. Evol. *31*, 201–211. https://doi.org/10.1093/molbev/mst190.
23. Pérez-Guijarro, E., Yang, H.H., Araya, R.E., El Meskini, R., Michael, H.T., Vodnala, S.K., Marie, K.L., Smith, C., Chin, S., Lam, K.C., et al. (2020). Multimodel preclinical platform predicts clinical response of melanoma

to immunotherapy. Nat. Med. *26*, 781–791. https://doi.org/10.1038/s41591-020-0818-3.

24. Gruen, C., Yang, H.H., Sassano, A., Wu, E., Gopalan, V., Marie, K.L., Castro, A., Rashidi Mehrabadi, F., Wu, C.H., Church, I., et al. (2023). Melanoma clonal subline analysis uncovers heterogeneity-driven immunotherapy resistance mechanisms. Preprint at bioRxiv. https://doi.org/10.1101/2023.04.03.535074.
25. Baserga, R. (1991). Growth regulation of the pcna gene. J. Cell Sci. *98*, 433–436. https://doi.org/10.1242/jcs.98.4.433.
26. Pabla, S., Seager, R.J., Van Roey, E., Gao, S., Hoefer, C., Nesline, M.K., DePietro, P., Burgher, B., Andreas, J., Giamo, V., et al. (2021). Integration of tumor inflammation, cell proliferation, and traditional biomarkers improves prediction of immunotherapy resistance and response. Biomark. Res. *9*, 56. https://doi.org/10.1186/s40364-021-00308-6.
27. Hansen, T.F. (1997). Stabilizing selection and the comparative analysis of adaptation. Evolution *51*, 1341–1351. https://doi.org/10.1111/j.1558-5646.1997.tb01457.x.
28. Chen, J., Swofford, R., Johnson, J., Cummings, B.B., Rogel, N., Lindblad-Toh, K., Haerty, W., Di Palma, F.D., and Regev, A. (2019). A quantitative framework for characterizing the evolutionary history of mammalian gene expression. Genome Res. *29*, 53–63. https://doi.org/10.1101/gr.237636.118.
29. Price, P.D., Palmer Droguett, D.H., Taylor, J.A., Kim, D.W., Place, E.S., Rogers, T.F., Mank, J.E., Cooney, C.R., and Wright, A.E. (2022). Detecting signatures of selection on gene expression. Nat. Ecol. Evol. *6*, 1035–1045. https://doi.org/10.1038/s41559-022-01761-8.
30. Zhou, S., Liang, Y., Zhang, X., Liao, L., Yang, Y., Ouyang, W., and Xu, H. (2020). Sharpin promotes melanoma progression via rap1 signaling pathway. J. Invest. Dermatol. *140*, 395–403.e6. https://doi.org/10.1016/j.jid.2019.07.696.
31. Semenov, M.V., Habas, R., MacDonald, B.T., and He, X. (2007). Snapshot: noncanonical wnt signaling pathways. Cell *131*, 1378. https://doi.org/10.1016/j.cell.2007.12.011.
32. Webster, M.R., Kugel, C.H., III, and Weeraratna, A.T. (2015). The wnts of change: How wnts regulate phenotype switching in melanoma. Biochim. Biophys. Acta *1856*, 244–251. https://doi.org/10.1016/j.bbcan.2015.10.002.
33. Chauhan, J.S., Hölzel, M., Lambert, J.-P., Buffa, F.M., and Goding, C.R. (2022). The mitf regulatory network in melanoma. Pigment Cell Melanoma Res. *35*, 517–533. https://doi.org/10.1111/pcmr.13053.
34. Rambow, F., Marine, J.-C., and Goding, C.R. (2019). Melanoma plasticity and phenotypic diversity: therapeutic barriers and opportunities. Genes Dev. *33*, 1295–1318. https://doi.org/10.1101/gad.329771.119.
35. Rambow, F., Rogiers, A., Marin-Bejar, O., Aibar, S., Femel, J., Dewaele, M., Karras, P., Brown, D., Chang, Y.H., Debiec-Rychter, M., et al. (2018). Toward minimal residual disease-directed therapy in melanoma. Cell *174*, 843–855.e19. https://doi.org/10.1016/j.cell.2018.06.025.
36. Hogan, P.G., Chen, L., Nardone, J., and Rao, A. (2003). Transcriptional regulation by calcium, calcineurin, and nfat. Genes Dev. *17*, 2205–2232. https://doi.org/10.1101/gad.1102703.
37. Ninova, M., Fejes Tóth, K., and Aravin, A.A. (2019). The control of gene expression and cell identity by h3k9 trimethylation. Development *146*, dev181180. https://doi.org/10.1242/dev.181180.
38. Wend, P., Holland, J.D., Ziebold, U., and Birchmeier, W. (2010). Wnt signaling in stem and cancer stem cells. Semin. Cell Dev. Biol. *21*, 855–863. https://doi.org/10.1016/j.semcdb.2010.09.004.
39. Pagadala, M., Sears, T.J., Wu, V.H., Pérez-Guijarro, E., Kim, H., Castro, A., Talwar, J.V., Gonzalez-Colin, C., Cao, S., Schmiedel, B.J., et al. (2023). Germline modifiers of the tumor immune microenvironment implicate drivers of cancer risk and immunotherapy response. Nat. Commun. *14*, 2744. https://doi.org/10.1038/s41467-023-38271-5.
40. Jiang, P., Gu, S., Pan, D., Fu, J., Sahu, A., Hu, X., Li, Z., Traugh, N., Bu, X., Li, B., et al. (2018). Signatures of T cell dysfunction and exclusion predict cancer immunotherapy response. Nat. Med. *24*, 1550–1558. https://doi.org/10.1038/s41591-018-0136-1.
41. Love, M.I., Huber, W., and Anders, S. (2014). Moderated estimation of fold change and dispersion for rna-seq data with deseq2. Genome Biol. *15*, 550. https://doi.org/10.1186/s13059-014-0550-8.
42. Meierjohann, S., and Bertolotto, C. (2024). Messing with cancer therapy: how the melanoma phenotype predicts checkpoint inhibitor response. Signal Transduct. Target. Ther. *9*, 76. https://doi.org/10.1038/s41392-024-01785-5.
43. Baggiolini, A., Callahan, S.J., Montal, E., Weiss, J.M., Trieu, T., Tagore, M.M., Tischfield, S.E., Walsh, R.M., Suresh, S., Fan, Y., et al. (2021). Developmental chromatin programs determine oncogenic competence in melanoma. Science *373*, eabc1048. https://doi.org/10.1126/science.abc1048.
44. Gopalan, V., Day, C.-P., Pérez-Guijarro, E., Chin, S., Ebersole, J., Smith, C., Simpson, M., Sassano, A., Alves Constantino, M., Wu, E., et al. (2022). Comprehensive single-cell transcriptomic analysis of embryonic melanoblasts uncovers lineage-specific mechanisms of melanoma metastasis and therapy resistance. Preprint at bioRxiv. https://doi.org/10.1101/2022.10.14.512297.
45. Martincorena, I., Raine, K.M., Gerstung, M., Dawson, K.J., Haase, K., Van Loo, P., Davies, H., Stratton, M.R., and Campbell, P.J. (2017). Universal patterns of selection in cancer and somatic tissues. Cell *171*, 1029–1041.e21. https://doi.org/10.1016/j.cell.2017.09.042.
46. Cooper, N., Thomas, G.H., Venditti, C., Meade, A., and Freckleton, R.P. (2016). A cautionary note on the use of ornstein uhlenbeck models in macroevolutionary studies. Biol. J. Linn. Soc. Lond. *118*, 64–77. https://doi.org/10.1111/bij.12701.
47. Wu, T., Hu, E., Xu, S., Chen, M., Guo, P., Dai, Z., Feng, T., Zhou, L., Tang, W., Zhan, L., et al. (2021). clusterprofiler 4.0: A universal enrichment tool for interpreting omics data. Innovation (Camb) *2*, 100141. https://doi.org/10.1016/j.xinn.2021.100141.
48. Noonan, F.P., Zaidi, M.R., Wolnicka-Glubisz, A., Anver, M.R., Bahn, J., Wielgus, A., Cadet, J., Douki, T., Mouret, S., Tucker, M.A., et al. (2012). Melanoma induction by ultraviolet a but not ultraviolet b radiation requires melanin pigment. Nat. Commun. *3*, 884. https://doi.org/10.1038/ncomms1893.
49. Anders, S., and Huber, W. (2010). Differential expression analysis for sequence count data. Genome Biol. *11*, R106. https://doi.org/10.1186/gb-2010-11-10-r106.
50. Robinson, M.D., McCarthy, D.J., and Smyth, G.K. (2010). edger: a bioconductor package for differential expression analysis of digital gene expression data. Bioinformatics *26*, 139–140. https://doi.org/10.1093/bioinformatics/btp616.
51. Zappia, L., Phipson, B., and Oshlack, A. (2017). Splatter: simulation of single-cell rna sequencing data. Genome Biol. *18*, 174. https://doi.org/10.1186/s13059-017-1305-0.
52. Jiao, L., Liu, Y., Yu, X.-Y., Pan, X., Zhang, Y., Tu, J., Song, Y.-H., and Li, Y. (2023). Ribosome biogenesis in disease: new players and therapeutic targets. Signal Transduct. Target. Ther. *8*, 15. https://doi.org/10.1038/s41392-022-01285-4.

STAR★METHODS

KEY RESOURCES TABLE

REAGENT or RESOURCE	SOURCE	IDENTIFIER
Antibodies		
Mouse anti-mouse CTLA-4 (Clone 9D9)	Bio X Cell	Cat# BE0164; RRID: AB_10949609
Mouse IgG2b (Clone MPC-11)	Bio X Cell	Cat# BE0086; RRID: AB_1107791
Deposited data		
Single-cell RNA data of clonal sublines	This paper	GEO: GSE215963
Gene expression of mouse melanoma after anti-CTLA-4 treatment	This paper	GEO: GSE255484
Experimental models: Cell lines		
B2905 mouse melanoma cell line	Dr. Glenn Merlino (Also available in ATCC)	B2905 (ATCC cat# CRL-3476); RRID: CVCL_B0CG
Clonal subline of B2905, C1-C24	Dr. Glenn Merlino	B2905 C1 to C24
Software and algorithms		
Python version 3	Python Software Foundation	https://www.python.org
R version 4	The R Foundation	https://www.r-project.org/
EvoGeneX	Pal et al.[17]	https://github.com/ncbi/EvoGeneX
clusterProfiler	Wu et al.[47]	https://bioconductor.org/packages/release/bioc/html/clusterProfiler.html
DESeq2	Love et al.[41]	https://www.bioconductor.org/packages/release/bioc/html/DESeq2.html
Trisicell	Rashidi Mehrabadi et al.[15]	https://trisicell.readthedocs.io/
Analysis code	This paper	https://github.com/ncbi/nongenomic-evolution-of-tumor-subclones

EXPERIMENTAL MODEL AND SUBJECT DETAILS

For M4 melanoma model, pups of hepatocyte growth factor (HGF)-transgenic C57BL/6 mice received UV irradiation at postnatal day 3, and melanoma would emerge in 6 – 8 months. A melanoma was harvested from a male mouse to make B2905 cell line.[48] B2905 melanoma carries spontaneous hotspot mutations in *Kras*, *Gnaq*, and *Sf3b1*.[23] The M4 melanoma model for preclinical study was built by implanting B2905 cells into C57BL/6 mice subcutaneously.

The development of the 24 clonal sublines was described previously.[24] In brief, 24 single cells were randomly selected and isolated from the parental B2905 mouse melanoma line, which was generated[23] and cultured in our laboratory, by cell sorting without any labeling. They were expanded in culture to become individual clonal sublines, C1 to C24. Cells were considered low quality and removed from the dataset if they had fewer than 500,000 reads, fewer than 1,000 genes detected, or if over 20% of the genes detected were mitrochondrial genes.[15] We further remove the cells that were missing data for any of the sublines, keeping only those that had at least one non-zero replicate for every subline. Analyses of whole exome, whole transcriptomics, and single-cell full transcripts were also described by.[24]

For the preclinical study of B2905 melanoma response to anti-CTLA-4 (“Genes with adaptively evolving expression underline therapeutic responses”), wildtype female C57BL/6 at the age of 6–8 weeks old were purchased from The Charles River at NCI Frederick. Mice at Laboratory Animal Science Program, National Frederick Laboratory for Cancer Research were housed in micro-isolator and individually ventilated cages supplied with acidified water and fed 5053 Irradiated Picolab Rodent Diet 20 lab diet. Temperature for laboratory mice in our facility is maintained between 18–23° C with 40–60% humidity. All animal procedures are conducted in laminar flow hoods. All personnel are required to wear scrubs and lab coat, mask, hair net, shoe covers, and disposable gloves upon entering the animal rooms. A 12 light/12 dark cycle was used for the mice. The animal study protocol (16-007) was approved by the Animal Care and Use Committee at NCI Frederick.

In all, 1.0×10^6 B2905 cells were implanted into the flank of 40 female C57Bl/6 mice, aged 6 – 8 weeks. The tumor size was measured twice a week. When tumors reached 75 mm^3 of size by average, mice were randomized into three groups to receive treatment of anti-CTLA-4 (Bio X Cell Cat.No. BE0164, clone 9D9; 30 mice), IgG2b isotype control (Bio X Cell Cat.No. BP0086, clone MPC-11; 5 mice), or left untreated (5 mice). The antibody was given to mice at 10 mg/kg i.v., twice a week for two consecutive weeks. After

the completion of antibody dosing, tumors with size approximately unchanged or decreasing at the next three measurements were identified as stable disease or responder tumors, respectively, and harvested. For those with size continuously increasing at the next three measurements, they were identified as non-responder and harvested at designated size. In any group, when the tumor reached 2000 mm^3 or ulcerated, or mice showed behavior of sickness, the endpoint was achieved, the mice would be euthanized by trained personnel with carbon dioxide inhalation in a euthanasia chamber, following the procedure in our animal study protocol. 25 tumors were harvested before reaching the endpoint and subjected to RNA sequencing. The rest were allowed to reach the endpoint for observing therapeutic efficacy. After euthanization, the tumor would be harvested for flash freezing in liquid nitrogen or fixation in paraformaldehyde, and the mouse would be examined by necropsy. The flash-frozen tumor would be processed for RNA sequencing.

METHOD DETAILS

Determining adaptive genes with Brownian motion and Ornstein-Uhlenbeck models

We use three stochastic models to determine adaptivity: a Brownian motion model, an Ornstein-Uhlenbeck model with a single optimum, and an Ornstein-Uhlenbeck model with two optima. These models describe the change of expression for a gene for a subline over time. There is no assumption of interaction or admixing among the "species." Brownian motion describes a stochastic process where the gene expression values change by a random value from a normal distribution at each time step t:

$$dX_i(t) \sim \mathcal{N}\left(0, \sigma^2\right)$$

where X_i is the expression value of species i, and σ is the standard deviation of the normal distribution.

The Ornstein-Uhlenbeck model is a generalization of Brownian motion that includes a pull to an "optimum" value at each time step:

$$dX_i(t) = \alpha(\theta_i - X_i(t))dt + \sigma dB(t)$$

where θ_i is the optimum value for species i, α is the influence of the optimum on the change, and $dB(t)$ is change from Brownian motion. When $\alpha = 0$, this model simplifies to Brownian motion.

We extend this to include multiple replicate values for each gene. To model this, we add a noise term to the species value:

$$dY_{i,k}(t) = X_i(t) + \varepsilon_{i,k}$$

where $Y_{i,k}$ is the replicate value for species i, replicate k, $\varepsilon_{i,k} \sim \mathcal{N}\left(0, \gamma\sigma^2\right)$ is a Gaussian variable with mean 0 and variance $\gamma\sigma^2$, which represents the within-species variability.

Parameters σ, α, θ_i, and γ are estimated using the maximum likelihood procedure described in the original EvoGeneX study.[17] Initial values of the parameters α and γ were set to 0.1 and 0.01, respectively, as they are shown to work well in the original study.[17] Although this method assumes that replicates of a species are normally distributed, we show using simulation studies that it can still be used to predict adaptivity of single-cell data, which is known not to be normally distributed.

Simulation studies

We perform simulation experiments in order to show that EvoGeneX[17] is appropriate for single-cell cancer data. We do this by simulating expression data under neutral, constrained, and adaptive models with high levels of noise that resemble the single-cell RNA sequence data we analyze.

In order to simulate single-cell data undergoing different modes of evolution, we first simulate the mean value of each species by running a Brownian motion (BM) or Ornstein-Uhlenbeck (OU) process down the tree with the root value fixed. We use the R library OUwie to model BM and OU processes. Rather than create replicates using a normal distribution as previously used to simulate bulk data,[17] we draw replicates from either a Poisson or a negative binomial distribution, which are more appropriate to simulate single-cell RNA sequence data.[49–51] The Poisson distribution has both mean and variance equal to the species value, giving the expression value of species i, replicate k at time t as

$$Y_{i,k}(t) \sim \text{Pois}(X_i(t)).$$

Where $X_i(t)$ is the mean expression value of that species simulated by the BM or OU process.

The variance represents the within-species variation (here, within-subline variation). The Poisson distribution does not have a parameter to control the variance separately from the mean, so using this distribution we cannot determine how the within-species variation affects the results. The negative binomial distribution introduces a dispersion parameter r, which affects the variance along with the mean. The expression value of species i, replicate k at time t is

$$Y_{i,k}(t) \sim \text{NB}(X_i(t), r).$$

The variance of the negative binomial is $X_i(t) + \frac{X_i(t)^2}{r}$, so as r increases, the within-subline variation decreases. The variance of the negative binomial distribution will always be greater than that of the Poisson distribution. This increase in noise in the data suggests that the genes with adaptive expression under the negative binomial model will be harder to predict.

We run simulations over the mutation tree from the 23 subline experiments with the highly aggressive and resistant (HA-R) regime and use parameter values estimated from the data. We set the expression level at the root to be 150, approximately equal to the mean of the expression values of all the replicates in the single-cell dataset. We vary σ^2 between 0.1%, 1%, and 10% of the expression at the root (0.15, 1.5, and 15) and α between 0.125, 1, and 8, which were chosen based on the simulations in Pal et al.[17] High σ^2 values represent high between-subline variation, and high α values represent a strong pull to the optimum value. We vary θ_1/θ_0 between 1.02, 1.04, 1.06, 1.08, and 1.1. The θ values are equidistant from the root value and θ_1 is higher and θ_0 is lower than the root value, respectively. Low θ_1/θ_0 values represent instances where the optima values are very similar, making the different harder to detect. For the negative binomial distribution, we vary r between 100, 150, and 200, where increasing values corresponds to decreasing within-subline variation.

We generate three types of data: 1) neutral data using BM (9 parameter combinations), 2) constrained data using an OU process with a single optimum (27 parameter combinations), and 3) adaptive data using an OU process with two optima using the HA-R regime (135 parameter combinations). For each combination of parameters, we simulate 100 genes, each with at most eight replicates with each having a 10% chance of drop-out to resemble the missing data in the real dataset.

Over every dataset, we run EvoGeneX with BM, OU with one optima, and OU with two optima. Running OU processes over the neutral data demonstrates the false positive rate. Running an OU process with a single optimum over data simulated as constrained and an OU process with two optima over the data simulated as adaptive demonstrates the true positive rate.

Random control runs

We test how many genes are predicted as adaptive when sublines are selected at random in order to confirm that our results are due to adaptive signal and not noise. In order to do this, we ran EvoGeneX over 50 randomly selected groups of three sublines, excluding the sublines in HA-R and SA-S, as we expect those sublines to have strong adaptive signals. We show the resulting distribution of the number of genes predicted to have adaptive expression in the random runs in Figure S3.

Clustering of genes with adaptive expression

We perform k-means clustering on the genes with adaptive expression in at least one of the three subline groups we analyzed. In order to do this, we assign each gene a value for each group based on the q-value for that regime, resulting in a set of three values for each gene. Specifically, for each regime r, a gene is assigned the following value:

$$v_r = \begin{cases} |\log_2 q| & \text{if adaptively upregulated in } r \\ -|\log_2 q| & \text{if adaptively downregulated in } r \\ 0 & \text{if not adaptive in } r \end{cases}$$

The genes are clustered based on these triplet values (i.e., the vector $[v_{\text{HA-R}}, v_{\text{SA-S}}, v_{\text{MA-S}}]$. We ran k-means clustering with 2 to 20 clusters and chose to use 12 clusters because it had the lowest silhouette score.

QUANTIFICATION AND STATISTICAL ANALYSIS

Function and pathway enrichment analysis

We use clusterProfiler[47] in R to determine enrichment of KEGG terms in genes using over-representation analysis. In the single-cell analysis, we determine enrichment of the genes with adaptive expression for each of the regimes. The background gene set for this analysis is all the genes in the single-cell data. In the bulk validation analysis, we use the genes that appear both in the single-cell data and the bulk data for the background set. We calculate q-values by correcting p-values with using Benjamini-Hochberg false discovery rate correction and consider pathways with a corrected q-value < 0.05 as significant.

Differential expression analysis

We used DESeq2[41] to perform differential expression analysis between post-treatment responder and non-responder tumors. We used as input the count matrix of the gene expression and ran DESeq2 with the default parameters. q-values were calculating by correcting p-values for multiple hypothesis testing using the Benjamini-Hochberg false discovery rate method and genes with q-values < 0.05 were considered significant.

dN/dS calculations

We estimate dN/dS on the bulk whole exome sequence data with a counting method. Because of the sparsity of gene-wise data, we only calculate dN/dS ratios over the entire genome. We calculate dN/dS for all sublines and the chosen sublines of each regime separately. We count the number of synonymous and nonsynonymous mutations across all genes in the chosen sublines. We then normalize these values by the expected number of synonymous and nonsynonymous sites in the data ($1/3$ of the sites are expected to be synonymous and $2/3$ of the sites are expected to be nonsynonymous) and divide the proportion of nonsynonymous sites by the proportion of synonymous sites.

1. The M4 mouse melanoma model represents RAS-mutated human melanoma with a transitory differentiation subtype. See Methods for detailed description.

2. Each clonal subline was grown from a single cell isolated from the B2905 cell line.[24]
3. While partitioning the tree to have more than two optima is possible, the addition of optima values to estimate reduces the power of the method, so here we only consider two optima.
4. SA-S was also enriched in the new Coronavirus pathway (hsa05171), but we found that this is caused by the enrichment in ribosomal genes[52] that constitute 89 out of 232 genes in this pathway so we do not include this pathway in the discussion.
5. In accordance with organism-specific formatting guidelines (https://www.ncbi.nlm.nih.gov/genbank/eukaryotic_genome_submission_annotation/), the mouse gene symbol begins with an uppercase letter, followed by lowercase letters, and human gene symbol uses all uppercase letters.